IOP Publishing Journal of Physics: Condensed Matter
J. Phys.: Condens. Matter **32** (2020) 195001 (9pp) https://doi.org/10.1088/1361-648X/ab6cc3

Vanadium doped polyoxometalate: induced active sites and increased hydrogen adsorption

Susan Meñez Aspera[1], Ryan Lacdao Arevalo[1,6], Hiroshi Nakanishi[1,2,3,5], Hideaki Kasai[1,2], Shinobu Sekine[4] and Hiroyuki Kawai[4]

[1] National Institute of Technology, Akashi College, 679-3 Nishioka, Uozumi, Akashi, Hyogo 674-8501, Japan
[2] Graduate School of Engineering, Osaka University, 2-1 Yamadaoka, Suita, Osaka 565-0871, Japan
[3] Institute of Industrial Science, The University of Tokyo, Meguro, Tokyo 153-8505, Japan
[4] Toyota Motors Corporation, 1200, Mishuku, Susuno, Shizuoka, 410-1193, Japan

E-mail: nakanishi@akashi.ac.jp

Received 5 November 2019, revised 13 December 2019
Accepted for publication 16 January 2020
Published 13 February 2020

Abstract

We analyzed the electronic and structural properties of an α-Keggin type molybdenum-based polyoxometalate (POM) [$[PMo_{12}O_{40}]^{3-}$] and its capacity for reduction reaction via H adsorption using *ab initio* calculations based on density functional theory (DFT). We also determined the change in the electronic properties brought about by vanadium substitutional doping, and its effect on the capacity of POM to adsorb H atom. We found that the optimal substitutional doping of four vanadium per one unit of POM is adequate to maintain its structural stability. Furthermore, increasing dopant concentration changes charge redistribution such that it induces charge transfer to an initially less active sites for H adsorption on pristine POM. This may increase the possibility of creating active sites from an initially inert H adsorption sites and allows for a higher density of H adsorption. This phenomenon could be relevant for chemical reactions that initially requires high number of pre-adsorbed H atoms.

Keywords: polyoxometalates, density functional theory, hydrogen adsorption, vanadium doping, first principles calculation

S Supplementary material for this article is available online

(Some figures may appear in colour only in the online journal)

1. Introduction

Polyoxometalates (POMs) are emerging materials that are of recent interest due to their wide variety of physical and chemical properties. These materials can act as a building block to form new materials. In general, POMs are class of compounds based on metal oxide building blocks with general formula $[MO_x]_n$, where M = Mo, W, V and sometimes Nb, and $x = 4$–7[2]. One of the broad subset groups of POM are heteropolyanions. They are metal oxides clusters that include heteroanions such as SO_4^{2-} and PO_4^{3-}. This group is the most studied subset of POM, particularly, the Keggin $[XM_{12}O_{40}]^{n-}$ and Wells–Dawson $[X_2M_{18}O_{62}]^{n-}$ anions (where M = W or Mo, X = is a tetrahedral template).

One important property of POM compounds that prompted development of new POM-based functional materials is its ability to tailor its redox properties. The redox properties of some Dawson type and Keggin type clusters can be tuned by incorporating different heteroatom or replacing one metal ion on the cluster shell. The tunability of the redox property was determined by factors such as the energy level, the shape of

[5] Author to whom any correspondence should be addressed.
[6] Present address: Department of Physics, University of San Carlos, Talamban Campus, Cebu City, Philippines

the lowest unoccupied molecular orbital, and the total charge of the anion, which are considered to be controlled via substitutional doping [3, 4]. An example is an experimental study showing POM with metal-oxo core containing transition metal atoms, Ru [5], Co [6] and Mn [7], which are efficient water oxidation catalysts. In particular, single site Ru-based POM with Keggin structures $[Ru^{III}(H_2O)XW_{11}O_{39}]^{-5}$ (X = Si, Ge) have been shown to be active for water oxidation [8]. Other applications of POM have been described in different fields such as catalysis [2, 8, 9] magnetism [10], and biological applications [11].

Tailoring electronic properties of POM via substitutional doping merits understanding of the electronic and structural property-changes brought about by the dopants. In line with this, we used theoretical analysis to understand the changes in the electronic and structural properties of molybdophosphate-based POM due to substitutional doping of vanadium metal oxo at different concentrations. The substitutional doping of a V^{+5} over the Mo^{+6} metal host will alter the charge distribution of the entire POM structure, and subsequently will affect the protonation properties of POM. This is important in the possible application of POM as an intermediate catalyst for the oxygen reduction reaction (ORR) process, where POM acts as an H carrier for the subsequent processes of ORR. $PMo_{12-x}V_x$ clusters are potential materials as chemically regenerative redox cathode (CRRC) catalysts for the proton exchange membrane fuel cell (PEMFC) [12]. In this kind of fuel cell, the liquid catalyst is reduced at the cathode, and re-oxidized in a 'regenerator' to form water via air bubbling [13]. As such, the capability of POM to be reduced and interact with H is an important factor to consider if it were to be used for this purpose. That ability to tune the reduction potential for the subsequent processes is therefore important and how these can be achieved is needed to be discussed.

2. Computational details

Density functional theory (DFT)-based first principles calculations were conducted using projector augmented wave (PAW) method [14] as implemented in the Vienna *ab initio* simulation package (VASP) codes [15, 16]. The generalized gradient approximation (GGA) with Perdew–Burke–Ernzerhof (PBE) [17] was used for the exchange-correlation approximation. In all calculations, the plane wave used has a cut-off energy of 500 eV [18], evaluated at a single Γ kpoint. The supercell used has a dimension of (25 Å × 25 Å × 25 Å) to ensure that no interaction between neighboring POM unit will occur due to the periodicity of the computational method used. Geometrical optimization was conducted until all the forces acting on each atom is less than 0.05 eV $Å^{-1}$. Dipole correction was included in all three vacuum directions, i.e. *x*-, *y*- and *z*-direction.

The POM structure used in this study is the α-Keggin structure with general formula $[PMo_{12}O_{40}]^{3-}$ (referred in this study as PMo_{12}), which is considered as the most stable structure of this formula unit. PMo_{12} is highly anionic with a net charge of $-3e$. The ionicity of PMo_{12} is attributed to its interaction with the environment, and in most situation due to solvation and in some crystal structures due to counterions. To account for the ionicity of PMo_{12}, we used Rb^+ counterions for simplicity. The use of Rb^+ as counterions in this study was based on recent reports of stable cubic structures of trirubidium molybdophosphate $Rb_3[PMo_{12}O_{40}]$ containing α-type Keggin $[PMo_{12}O_{40}]^{3-}$ anions and Rb^+ counterions located in orthogonally intersecting channels [19]. Rb^+ counterions were used for both PMo_{12} and V-doped PMo_{12}, namely: $[PMo_{11}V_1O_{40}]^{4-}$ (referred as $PMo_{11}V_1$), $[PMo_{10}V_2O_{40}]^{5-}$ (referred as $PMo_{10}V_2$), $[PMo_9V_3O_{40}]^{6-}$ (referred as PMo_9V_3), and $[PMo_8V_4O_{40}]^{7-}$ (referred as PMo_8V_4). The use of Rb^+ as counterions necessitates determining an optimal distance of the Rb atoms from the $PMo_{12-x}V_x$ clusters that would provide an optimal charge to the latter, i.e. an effective charged state of each the $PMo_{12-x}V_x$ cluster nearest to the assumed oxidation state. The effective charge of the $PMo_{12-x}V_x$ cluster is obtained from Bader charge analysis [20] and calculated by comparing the Bader charge with the atomic valence of neutral atoms. It is known that Bader charge analysis overestimates charge transfer, hence predicts a highly ionic interaction [21]. However, the focus of this study is the relative direction of charge transfer and its change due to alloying. In this sense, Bader charge analysis is usable. For analysis of the effective charge, negative values denotes electron gain while positive denotes electron loss. For example, it was determined that

Table 1. The average effective charge of PMo_{12} through Bader charge analysis and the average Mo–O bondlength.

Atom	Average effective charge (e)	Average Mo–O bond length (Å)
P	3.624	—
Mo	2.639	—
O_{ap1}	−1.459	2.46
O_{ap2}	−0.764	1.70
O_{bas1}	−0.970	1.92
O_{bas2}	−0.955	1.93

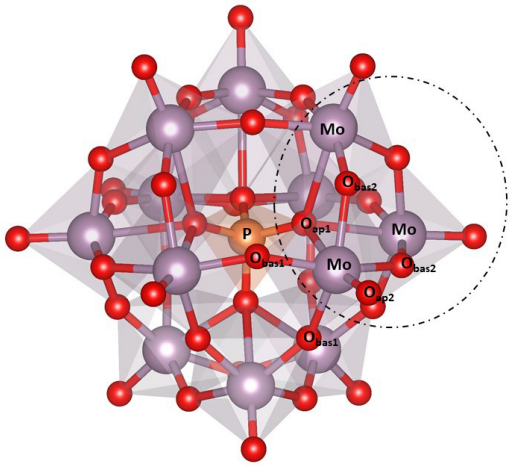

Figure 1. α-Keggin structure of POM with the formula unit $[PMo_{12}O_{40}]^{-3}$. A tri-octahedral group is highlighted, and the corresponding oxygen sites are labeled. Orange sphere represents P, light purple spheres represents Mo, and red spheres represents O. The VESTA code was used for visualization [1].

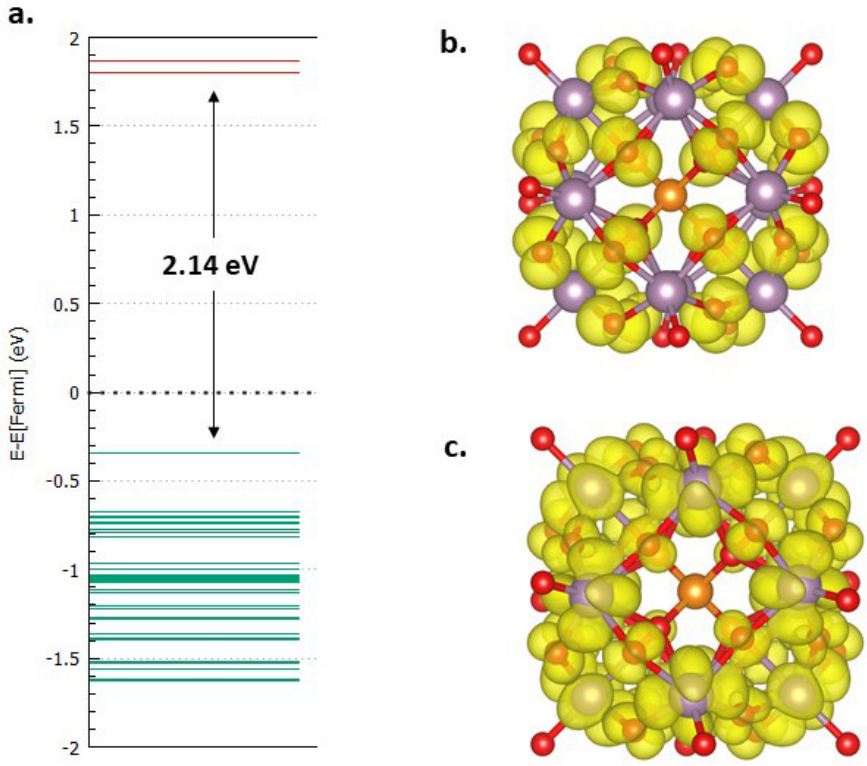

Figure 2. (a) The electron energy levels of POM near the chemical potential (dotted line). Charge distribution of the (b) HOMO and (c) LUMO level are indicated. The yellow region indicates the iso-surface of 0.005 e^- Å^{-3}. Orange sphere represents P, light purple spheres represents Mo, and red spheres represents O. The VESTA code was used for visualization [1].

the $3Rb^+$–PMo_{12} cluster distance of 7.84 Å will provide an optimal effective charge value of -2.813 e to PMo_{12}, which is the nearest to the assumed -3 e charge state of PMo_{12}. The Rb^+ counterions were then frozen at this distance for the succeeding calculations. The same method was used to induce charge to $PMo_{12-x}V_x$ clusters where the number of Rb^+ counterions increases to compensate for the changing anionic charge as the dopant concentration varies (supplementary information (stacks.iop.org/JPhysCM/32/195001/mmedia)). In all calculations involving optimization of the structure, the reference core P atom and the Rb counterions were fixed while the other atoms were allowed to move. The valence electrons used to represent each component atoms are $4s^2\ 4p^6\ 5s^1\ 4d^5$ for Mo, $3s^2\ 3p^6\ 3d^4\ 4s^1$ for V, $3s^2\ 3p^3$ for P and $2s^2\ 2p^4$ for O.

3. Results and discussions

3.1. The POM unit

The α-Keggin structure of PMo_{12} is composed of 12 vertex and edge-sharing MoO_3 octahedral units held together by a central PO_4^{3-} tetrahedral (figure 1). The 12 MoO_3 octahedral units are in a tri-octahedral groups connected to a common O (a 4-coordinated O labelled as O_{ap1}) of the PO_4^{3-} tetrahedral. In each of the tri-octahedral groups, the 2-coordinated O atoms that links each member of the tri-octahedral group is labelled as O_{bas1} and the 2-coordinated O atoms that link a tri-octahedral group to other tri-octahedral groups is labeled as O_{bas2}. The 12 vertex O atoms that are singly coordinated and directly connected to a metal atom are labeled as O_{ap2}. So basically, there are four types of O atoms in one PMo_{12} unit structure: two basal oxygens (labelled as O_{bas1}, O_{bas2}) and two apical oxygens (labelled as O_{ap1} and O_{ap2}). Each type of oxygen atoms has different charges according to Bader charge analysis. The largest belongs to the 4-coordinated O_{ap1} followed by the 2-coordinated basal oxygen atoms (table 1) where O_{bas1} has slightly higher effective charge than O_{bas2}. The O basal atoms are important for the reduction of PMo_{12} through H adsorption. The Mo–O bondlength for the same type of O atom slightly differs from each other with Mo–O_{bas2} distance ranging from 1.86 Å to 2.01 Å (for Mo–O_{bas1} it is 1.85 Å–2.01 Å), Mo–O_{ap1} ranging from 2.43 Å to 2.49 Å, and Mo–O_{ap2} ranging from 1.69 Å–1.71 Å. The average Mo–O bondlength with the different types of O atoms are also found in (table 1). From here, it can be observed that the length of the Mo–O distance is proportional to the coordination number of O, i.e. higher number of O coordination entails longer Mo–O bond length.

Figure 2 shows the energy level distribution plot of PMo_{12} near the HOMO-LUMO level. PMo_{12} has non-spin polarized energy levels with a bandgap of around 2.14 eV. The HOMO level is doubly degenerate composed mostly of the *p orbitals* of the O basal atoms (figure 2(b)). On the other hand, the LUMO and the LUMO+1 distribution is mostly composed of the *d orbitals* of the metal Mo and *p orbitals* of O basal atoms (figure 2(c)). Due to the non-uniformity of the O basal atom

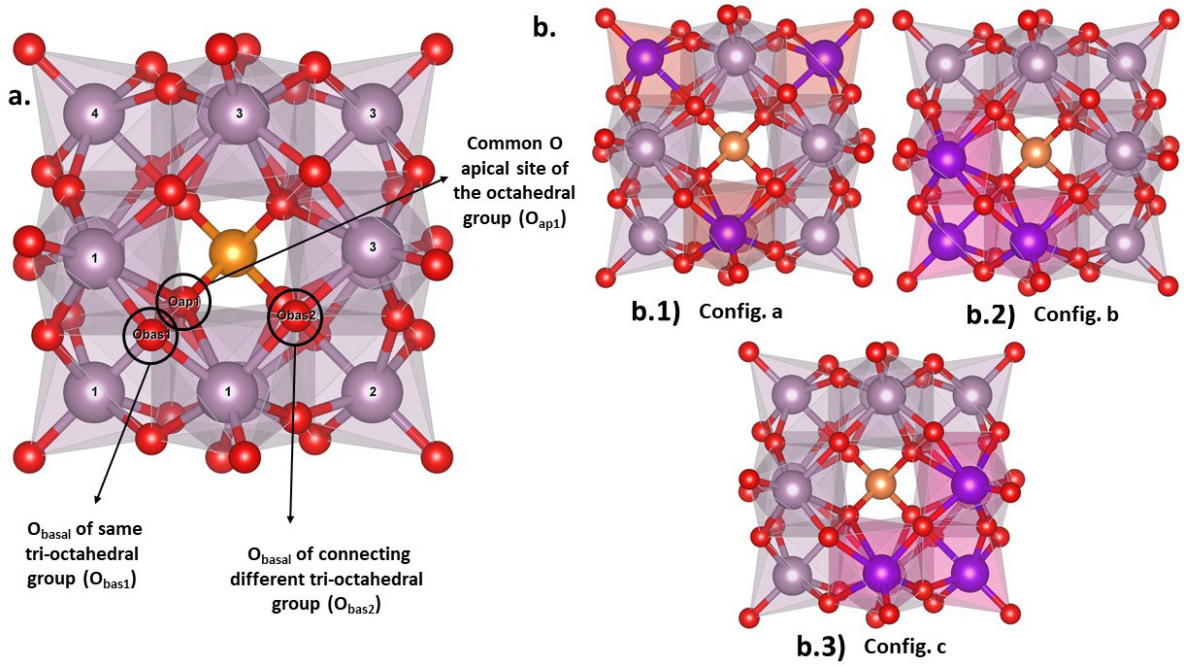

Figure 3. V substitutional doping on PMo_{12}. The doping position for different V doping configurations are depicted in (a). The numbers indicate MoO_3 octahedral that belong to the same tri-octahedral group. To sample, the doping configurations for three Vanadium dopants are depicted in (b). In (b.1) configuration A, the V dopants are at different tri-octahedral groups. In (b.2) configuration B, the V dopants are on the same tri-octahedral group coordinated to the same O_{ap1} atom. In (b.3) configuration C, the dopants are on next nearest Mo position but on different tri-octahedral groups. Orange sphere represents P, light purple spheres represents Mo, purple spheres represents V and red spheres represents O. The VESTA code was used for visualization [1].

charges, H adsorption on similar O basal sites will slightly vary with relatively small energy differences.

3.2. Vanadium doped POM

Changing the octahedral metal core with another of different oxidation state can tune the properties of POM towards specific functions. In this study, we used vanadium as substitutional dopants and evaluate the change in the structural and electronic properties of PMo_{12}. The substitutional dopant V^{+5} has a lower oxidation state than the host Mo^{+6}. The difference in the oxidation state of octahedral metal core will lead to a varying charged state, $[PMo_{12-x}V_x]^{(3+x)-}$. The 12 Mo sites are in equivalent positions in the α-Keggin structure of PMo_{12}. Therefore, the relative position of the V dopants with each other was used to determine the possible doping configurations (figure 3), which was done for different V-doping concentrations. Each Mo octahedral belongs to a tri-octahedral group through a common O_{ap1}. Each tri-octahedral group is linked to another tri-octahedral group via O_{bas2} (figure 3(a)). And each Mo octahedral of the same tri-octahedral group is linked via another O_{bas1}. We therefore based the doping sites on the uniqueness of these interactions and determined three possible doping configurations: (a) the V dopants are substituted on Mo atoms that are not nearest neighbors and belongs to different tri-octahedral groups (figure 3(b.1)), (b) the V dopants substituted on Mo atoms that belongs to the same tri-octahedral group (figure 3(b.2)), and (c) the V dopants are substituted on next nearest neighbor Mo atoms but belongs to different tri-octahedral groups (figure 3(b.3)).

Table 2. Relative energy of different configurations for different dopant concentrations.

	Energy relative to Config. A(eV)		
Configurations	$PMo_{10}V_2$	PMo_9V_3	PMo_8V_4
Config. A	0	0	0
Config. B	0.036	0.140	0.134
Config. C	0.076	0.195	0.234

Table 2 shows the relative energy of each configurations for the different dopant concentration, $PMo_{12-x}V_x$ where $x = 2$–4. It is observed here that Config. a, where the V dopants are substituted for Mo sites that belongs to different tri-octahedral groups and are far from other dopants, is the least energy configuration for all dopant concentrations. Furthermore, there is an increase in the relative energy for near-neighbor dopants as the number of dopants increases. Further increase in dopant concentration allows for occupation of near neighbor dopants, thereby increasing the relative energy of the system.

The formation energy of V doping for the most stable configuration at different dopant concentration was evaluated to determine the stability of the structure. The formation energy is defined as:

$$E_{\text{form}} = \frac{\{E_{((x+3)\text{Rb}-\text{PMo}_{12-x}\text{V}_x)} - [E_{(3\text{Rb}-\text{PMo}_{12})} + (x)(E_{\text{iso}_{\text{Rb}}} + \mu_{\text{V}} - \mu_{\text{Mo}})]\}}{x} \quad (1)$$

where $E_{((x+3)\text{Rb}-\text{PMo}_{12-x}V_x)}$ is the energy of the $PMo_{12-x}V_x$ with $(x+3)$ Rb^+ counterions, $E_{(3\text{Rb}-\text{PMo}_{12})}$ is the energy of PMo_{12} with 3 Rb^+ counterions, μ_{V} and μ_{Mo} are the chemical potential of V and M, respectively, obtained from the cohesive

Table 3. Formation energy of Vanadium doping per number of V dopants and average change in O atom charge for different dopant concentrations. The change in O atom charge is averaged per site and compared with undoped POM. Negative values of formation energy pertain to stability. Negative values of the change on O atom charge pertains to increase in electron number, on the other hand, positive values pertain to decrease in electron number.

		Average change in O atom charge relative to undoped POM (e/atom)			
Structure	Formation Energy (eV/atom)	O_{bas1}	O_{ap2}	O_{ap1}	O_{bas2}
$PMo_{11}V_1$	−1.246	−0.003	−0.031	0.002	−0.007
$PMo_{10}V_2$	−1.291	−0.002	−0.060	0.005	−0.018
PMo_9V_3	−1.607	−0.009	−0.083	0.008	−0.027
PMo_8V_4	−2.082	−0.006	−0.099	0.010	−0.044

energy per atom of its bulk structures (in this case, BCC structures), $E_{iso_{Rb}}$ is the energy of an isolated Rb atom in a large box, and x is the number of V dopant. Table 3 shows the formation energy of the most stable configuration, i.e. Config. A, for $PMo_{12-x}V_x$, where $x = 1$–4. It is observed here that as the number of V dopants increase up to 4 per $PMo_{12-x}V_x$ unit, the stability also increases implying favorable dopant formation. However, increasing the dopants further than 4 V allows occupation of dopants at the same tri-octahedral group, which decreases the stability of the system relative to PMo_8V_4. This implies that PMo_7V_5 and PMo_6V_6 or even high number of V dopants could have lower stability than PMo_8V_4. The instability of PMo_7V_5 and higher number of V doping was experimentally verified. PMo_7V_5 and higher number of V dopants are hard to synthesize, and if successfully synthesized, the resulting structure breaks down within a few weeks [22]. Furthermore, previous studies show that Mo and V addendum are very labile and can easily move in and out of the POM structure, in which the equilibrium mixtures contain different POM anions, phosphate and free vanadium [12]. This labile property of the V dopants, presence of free vanadium at equilibrium systems and the relative instability of PMo_7V_5 (and higher V dopants), could contribute to the decomposition of $PMo_{12-x}V_x$ with more than 5 V dopants.

Table 3 also shows the average change of O atom charges per O site relative to PMo_{12}. It is observed here that as the number of V dopants increases, the change in the average effective charge similarly increases. This could be attributed to the increasing charge state of POM for every additional V dopant. It can also be observed here that the 1-coordinated O_{ap2} has the highest charge gain per additional V dopant. However, the change in the charge distribution on each O atom depends on its relative position from the V dopants. To sample, figure 4 shows the change in charge of the O atoms of PMo_9V_3 relative to the undoped PMo_{12}. It is observed here that the O atoms directly coordinated to the V dopants have less or minimally increased their effective charges as compared with the O atoms far from the V dopants. Also, the highest gain in charge are the O_{ap2} that are coordinated to the Mo atoms. The increase in O effective charges due to the difference in the oxidation state of the dopant possibly enhances the interaction between the O atoms and the metal atoms thus increasing the stability of the system.

The charge distribution projected onto the HOMO and LUMO of PMo_{12} and $PMo_{12-x}V_x$ are shown in figures 5(a)–(e).

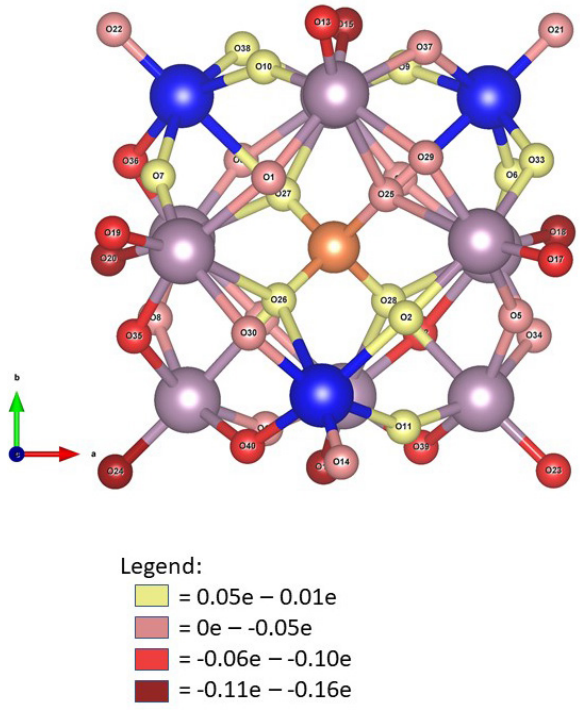

Figure 4. Change in the O charge distribution of PMo_9V_3 relative to PMo_{12}. Range of negative values of O charge entails increase in charge as compare with PMo_{12} for the same O site. On the other hand, positive values show decrease in electron number. Orange sphere represents P, light purple spheres represents Mo, blue spheres represents V and all other spheres represents O atoms. The VESTA code was used for visualization [1].

It is observed here that the LUMO electron distribution are mostly from *d orbitals* of Mo and V and the π *bonding orbital* of Mo–O_{bas} and V–O_{bas}, for both doped and undoped systems. For PMo_{12}, the HOMO distribution of POM is mostly from the *p orbitals* of O_{bas}, and the O_{ap2} *p orbitals* are located at lower energy levels. However, upon introduction of V dopants, emergent states from the O_{ap2} *p orbitals* appears at the HOMO level. These could be attributed to the difference in the oxidation states and electronegativity of the host and the dopant atoms. Due to the higher electronegativity of the Mo atoms than V atoms, charge re-distribution occurs such that the distribution of changes along the vicinity of the Mo–O bond is higher than along the V–O bonds. The significance of Mo and V co-doping could be attributed to this redistribution of charges such that it activates the O_{ap2} atoms as active sites

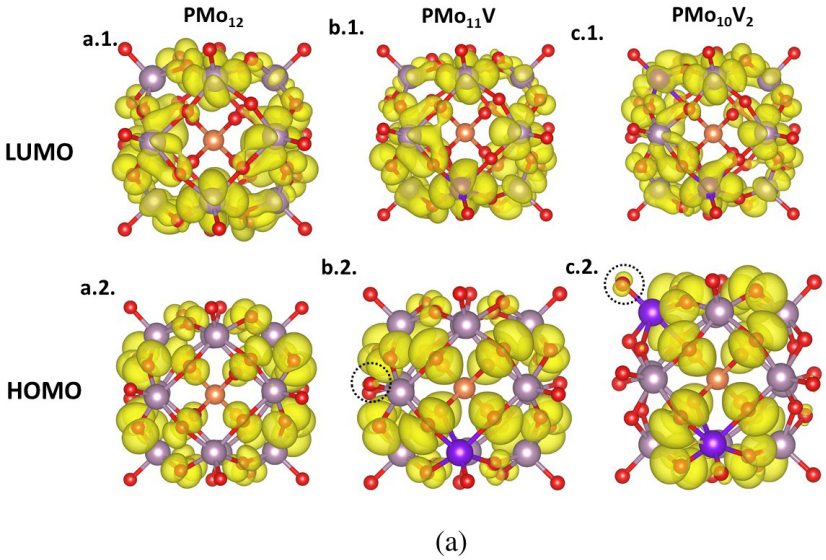

Figure 5. Charge distribution of the HOMO-LUMO states for the PMo_{12} and $PMo_{12-x}V_x$ with Rb^+ counterions: (a.1) LUMO and (a.2) HOMO of PMo_{12}; (b.1) LUMO and (b.2) HOMO of POM of $PMo_{11}V_1$; (c.1) LUMO and (c.2) HOMO of POM of $PMo_{10}V_2$; (d.1) LUMO and (d.2) HOMO of POM of PMo_9V_3; and (e.1) LUMO and (e.2) HOMO of POM of PMo_8V_4. The emergent states at the O_{ap2} orbitals are highlighted in the charge distribution particularly at the HOMO, as indicated by the dotted circle. The iso-surface value is 0.005 e^- Å^{-3}. The VESTA code was used for visualization [1].

to participate in the reaction by inducing O_{ap2} states at the frontier orbitals.

3.3. H adsorption on POM and V-doped POM

The effect of V doping on PMo_{12} for molecular interaction was analyzed through H adsorption. We explored the possible changes in the potential energy for redox reaction on POM by analyzing the effect of different V dopant concentration on the reduction of POM through H adsorption. The change in reduction potential of POM can determine its capability for oxidation reaction, specifically for the formation of H_2O from ORR via the cathode site of PEMFC.

H atom was adsorbed on O sites of PMo_{12} and $PMo_{12-x}V_x$ with the highest effective charge based on Bader volume distribution for each type of O atom, i.e. O_{bas1}, O_{bas2}, O_{ap2}, and O_{bas} nearest a V dopant. The H adsorption energy was obtained using

$$E_{\text{ads}} = E_{(x+3)\text{Rb}-\text{PMo}_{12-x}\text{V}_x-\text{H}} - \left(E_{(x+3)\text{Rb}-\text{PMo}_{12-x}\text{V}_x} + \frac{1}{2}E_{\text{H}_2}\right). \quad (2)$$

Where $E_{(x+3)\text{Rb}-\text{PMo}_{12-x}\text{V}_x-\text{H}}$ is the energy of $PMo_{12-x}V_x$ with x number of V dopants and an adsorbed H, $E_{(x+3)\text{Rb}-\text{PMo}_{12-x}\text{V}_x}$ is the energy of POM with an x number of V dopants and E_{H_2} is the energy of an isolated hydrogen molecule. Table 4 shows the H adsorption energy on the different O adsorption sites for varying number of V dopants. The effective charges of each O atom target adsorption site before H adsorption is also indicated. In general, we can see a weak H adsorption on the single coordinated O_{ap1} site as compared to the O_{bas} sites for each of the $PMo_{12-x}V_x$. It is also apparent that for PMo_{12} and $PMo_{11}V_1$, H adsorption on the O_{ap2} site is unstable. However, upon increasing of the number of V dopants, we can see a more attractive interaction of H on the apical site thereby increasing the possibility of allowing

Table 4. H adsorption on different O sites for changing number of V dopants. The highest effective charge per atom type was tested for H adsorption dependent on the sites. A negative effective charge indicates increase in charge distribution around the atom based on Bader volume partitioning as compared to the valence of an isolated atom. The adsorption energy of H atom is relative to isolated surface and hydrogen molecule. Negative values of adsorption energy pertain stability.

	PMo_{12}		$PMo_{11}V_1$		$PMo_{10}V_2$		PMo_9V_3		PMo_8V_4	
H position	Charge (e)	Adsorption energy (eV)	Charge (e)	Adsorption energy (eV)	Charge (e)	Adsorption energy (eV)	Charge (e)	Adsorption energy (eV)	Charge (e)	Adsorption energy (eV)
O_{bas1}	−0.984	−0.15	−0.992	−0.45	−1.001	−1.41	−1.006	−1.55	−1.014	−1.04
O_{bas2}	−0.981	−0.52	−0.983	−0.67	−0.995	−1.19	−1.000	−1.34	−1.066	−1.13
O_{ap2}	−0.794	—	−0.828	—	−0.854	−0.54	−0.879	−0.65	−0.950	−0.45
Near V dopant			−0.918	−0.73	−0.946	−1.12	−0.975	−1.35	−0.979	−1.27

'—' are unstable adsorption sites.

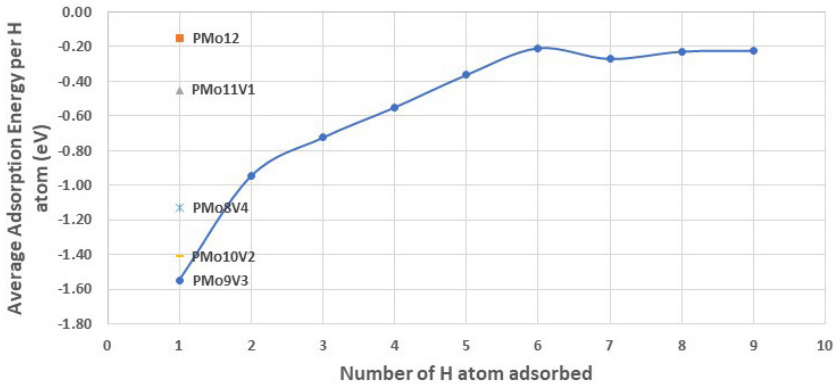

Figure 6. H adsorption energy per H atom on PMo_9V_3 for increasing number of H adsorbates. For PMo_9V_3, position of each H adsorption is based on the O atom with the highest effective charge through Bader charge analysis. The initial H adsorption for different number of V dopants is also indicated, where the values were obtained from the more stable adsorption sites.

the apical site to participate in the adsorption reaction. Also, as the number of V dopants increases, the H adsorption energy increases. This could also be attributed to the increase in the effective charges of the corresponding O atoms via increase of V dopants, enhancing its nucleophilic properties. An increase in the initial H adsorption translates to higher capacity for succeeding H adsorption (figure 6). Figure 6 shows the adsorption energy of increasing number of H atom adsorbed on the PMo_9V_3 system. The adsorption energy per H atom is calculated as:

$$E_{\text{ads\_}n\text{H}} = \left[E_{(x+3)\text{Rb}-\text{PMo}_{12-x}\text{V}_x-n\text{H}} - \left(E_{(x+3)\text{Rb}-\text{PMo}_{12-x}\text{V}_x} + \frac{n}{2}E_{\text{H}_2}\right)\right]/n \tag{3}$$

where $E_{(x+3)\text{Rb}-\text{PMo}_{12-x}\text{V}_x-n\text{H}}$ is the energy of n number of H atom adsorbed on $PMo_{12-x}V_x$. The O adsorption sites for each succeeding H adsorption is based on the highest O effective charges with the pre-adsorbed H atoms. According to figure 6, as the number of adsorbed H atom increases, the average adsorption energy per H atom decreases. In this case, at around 6 H atom, there is a significant decrease in the difference of adsorption energy per succeeding H atoms until it reaches a saturation point. This tendency is also expected for different concentration of V dopants where the initial H adsorption energy could determine the number of strongly bound H atom before it reaches saturation. In this case, increasing the number of V dopants could provide a high density of adsorbed H that could participate in the reaction. These results are in qualitative agreement with previous experimental investigations on the regenerative redox properties of PMo_9V_3 [13]. In these analysis, the number of H adsorbed in POM is described in terms of the number of the concentration of V^{+4} dopants. It was assumed that the regenerative mechanism of $PMo_{12-x}V_x$ clusters is attributed to the reduction of POM via the changing oxidation state of the Vanadium dopants from V^{+5} to V^{+4}, which are considered as first to accept electrons in electrochemical reactions. Results show that the catholyte potential decreases as the fraction of V^{+4} increases. Correlatively, this inverse tendency of decreasing catholyte potential with increasing fraction of V^{+4} corresponds to a decrease in H adsorption energy as the number of H increases. Furthermore, $[PMo_{12}O_{40}]^{3-}$ and $[PMo_{11}V_1O_{40}]^{4-}$ are known not to react with oxygen under mild condition [13]. This could be attributed to a low number of adsorbed H atoms, which could be attributed to a weaker initial H adsorption and the decrease in adsorption energy for the succeeding H atoms.

4. Summary

The effect of V doping on the change in the electronic properties of POM $[PMo_{12}O_{40}]^{3-}$ anions was analyzed using DFT-based calculations. We used the α-Keggin structure of PMo_{12} and included the effects of counterions using Rb^+ cations. Our results show that up to 4 V substitutional doping, the structures are most stable. Increasing the number of V dopants would allow for a 2 V-dopant occupation on the same tri-octahedral group, which would decrease the stability of the system relative to PMo_8V_4. Furthermore, V doping creates charge redistribution such that minimal increase in the additional charges were observed on the O atoms directly coordinated with the V dopants. The highest gain in charge through V substitutional doping are the singly-coordinated O_{ap2} atoms, particularly those that are coordinated to Mo of the octahedral group. This increase in charge allows for more probable interaction of H^+ ions on O_{ap2} thus allows for possibility of being active sites for H adsorption. With the increase in effective charge per O atom via changing the concentration of the V dopants, higher density of adsorbed H atoms is possible. This is relevant for reactions that requires high number of pre-adsorbed H atoms.

Acknowledgment

This work is supported in part by JST ACCEL Grant No. JPMJAC1501 'Creation of the Functional Materials on the Basis of the Inter-Element-Fusion Strategy and their Innovative Applications', MEXT Grant-in-Aid for Scientific Research (16K04876), JST CREST Innovative Catalysts and Creation Technologies for the Utilization of Diverse Natural Carbon Resources: *in situ* atomic characterization of catalytic reactions for the development of Innovative Catalysts (No. 17942262), and MEXT Grant-in-Aid for Scientific Research (15H05736). Some of the numerical calculations presented here were done using the computer facilities at the following

institutes: High Energy Accelerator Research Organization (KEK), Institute for Solid State Physics (ISSP, University of Tokyo), Yukawa Institute for Theoretical Physics (YITP, Kyoto University), and the National Institute for Fusion Science (NIFS).

ORCID iDs

Susan Meñez Aspera https://orcid.org/0000-0001-9922-831X
Ryan Lacdao Arevalo https://orcid.org/0000-0002-3251-6920
Hiroshi Nakanishi https://orcid.org/0000-0001-9843-1527
Hideaki Kasai https://orcid.org/0000-0003-3260-9446

References

[1] Momma K and Izumi F 2011 *J. Appl. Crystallogr.* **44** 1272–6
[2] Long D-L, Tsunashima R and Cronin L 2010 *Angew. Chem., Int. Ed. Engl.* **49** 1736–58
[3] López X, Bo C and Poblet J M 2002 *J. Am. Chem. Soc.* **124** 12574–82
[4] Eda K and Osakai T 2015 *Inorg. Chem.* **54** 2793–801
[5] Sartorel A, Carraro M, Scorrano G, Zorzi R D, Geremia S, McDaniel N D, Bernhard S and Bonchio M 2008 *J. Am. Chem. Soc.* **130** 5006–7
[6] Yin Q, Tan J M, Besson C, Geletii Y V, Musaev D G, Kuznetsov A E, Luo Z, Hardcastle K I and Hill C L 2010 *Science* **328** 342–5
[7] Al-Oweini R, Sartorel A, Bassil B S, Natali M, Berardi S, Scandola F, Kortz U and Bonchio M 2014 *Angew. Chem., Int. Ed. Engl.* **53** 11100
[8] Piccinin S and Fabris S 2015 *Inorganics* **3** 374
[9] Pope M T and Müller A 1991 *Angew. Chem., Int. Ed. Engl.* **30** 34–48
[10] Lehmann J, Gaita-Ariño A, Coronado E and Loss D 2007 *Nat. Nanotechnol.* **2** 312
[11] Rhule J T, Hill C L, Judd D A and Schinazi R F 1998 *Chem. Rev.* **98** 327–58
[12] Singh R, Shah A A, Potter A, Clarkson B, Creeth A, Downs C and Walsh F C 2012 *J. Power Sources* **201** 159–63
[13] Gunn N L O, Ward D B, Menelaou C, Herbert M A and Davies T J 2017 *J. Power Sources* **348** 107–17
[14] Blöchl P E 1994 *Phys. Rev.* B **50** 17953–79
[15] Kresse G and Furthmüller J 1996 *Phys. Rev.* B **54** 11169–86
[16] Kresse G and Furthmüller J 1996 *Comput. Mater. Sci.* **6** 15–50
[17] Perdew J P, Burke K and Ernzerhof M 1996 *Phys. Rev. Lett.* **77** 3865–8
[18] Monkhorst H J and Pack J D 1976 *Phys. Rev.* B **13** 5188–92
[19] Armand P, Granier D and van der Lee A 2007 *Acta Crystallogr.* E **63** i191
[20] Henkelman G, Arnaldsson A and Jónsson H 2006 *Comput. Mater. Sci.* **36** 354–60
[21] Fonseca Guerra C, Handgraaf J-W, Baerends E J and Bickelhaupt F M 2004 *J. Comput. Chem.* **25** 189–210
[22] JNMC Ltd 2019 *personal communication*